

New infrared emission of the NV centre in diamond: Zeeman and uniaxial stress studies

L J Rogers, S Armstrong, M J Sellars and N B Manson

Laser Physics Center, RSPHysSE, Australian National University, Canberra,
ACT 0200, Australia

E-mail: lachlan.rogers@anu.edu.au

Abstract. An emission band in the infrared is shown to be associated with a transition within the negative nitrogen-vacancy center in diamond. The band has a zero-phonon line at 1046 nm, and uniaxial stress and magnetic field measurements indicate that the emission is associated with a transition between 1E and 1A_1 singlet levels. Inter-system crossing to these singlets causes the spin polarisation that makes the NV^- centre attractive for quantum information processing, and the infrared emission band provides a new avenue for using the centre in such applications.

PACS numbers: 42.50.Ex, 42.62.Fi, 61.72.jn, 71.70.Ej, 71.70.Fk, 78.30.-j

Keywords: infrared emission, electronic structure, nitrogen-vacancy center

1. Introduction

The electronic structure of the negative nitrogen vacancy (NV^-) center in diamond gives it properties that are attractive for aspects of quantum information applications [1, 2, 3, 4, 5, 6, 7, 8]. One of the attractive features is the phenomenon of optically induced spin polarization of the $S = 1$ ground state [9, 10, 11]. It has been proposed that the polarization arises due to inter-system crossing from the excited triplet state to singlet levels, and decay back to the ground state with an overall change of spin. This process was thought to be non-radiative due to the emission intensity dependence on the level of spin polarisation [12], and there was no direct knowledge of the singlets involved. However, in this work infrared emission from the NV^- centre is reported and shown to be associated with the singlet levels. Spectral analysis of this emission has provided information about the polarising decay path and the electronic structure of the NV centre.

2. Observations

2.1. Emission spectrum

Two synthetic 1b diamond samples of different defect concentrations were used. Both were 2 mm cubes that had been irradiated and annealed to produce NV^- centers with concentrations of about $3 \times 10^{18} \text{ cm}^{-3}$ (“high” concentration) and about 10^{17} cm^{-3} (“low” concentration). Each of the samples had $\langle 110 \rangle$, $\langle \bar{1}10 \rangle$ and $\langle 100 \rangle$ faces. The samples were excited with a 532 nm laser at 100 mW and the emission at right angles was dispersed by a monochromator and detected on an ADC model 403L cooled germanium photodetector. A weak infrared emission band with a zero-phonon line (ZPL) at 1046 nm was observed, and the spectrum is shown in Figures 1 and 2. The characteristic NV^- emission has a higher energy ZPL at 637 nm and vibrational sidebands that extend beyond 1000 nm, the extreme low energy tail of which create the intensity baseline in Figure 1. Throughout this paper the emission from the 637 nm transition is referred to as “visible” in order to differentiate it from the infrared emission band.

At room temperature the infrared ZPL at 1046 nm was clearly discernible accompanied by a vibrational band, and at low temperature the features were clearer and dominated by the zero-phonon line. The linewidth was measured to be 0.3 nm (0.3 meV) in the lower concentrated sample, but was broadened significantly to 4 nm in the higher concentration sample. The vibrational sideband had similar integrated area to the ZPL (\mathcal{S} -coefficient ≈ 1) and was comprised of peaks shifted by 42.6 meV (344 cm^{-1}), 133 meV (1070 cm^{-1}) and 221 meV (1780 cm^{-1}) from the ZPL.

2.2. Magnetic field measurements

The intensity of both infrared and visible emission bands was found to vary with low magnetic fields, and the variation for the low concentration sample is shown in Figure 3 for fields between 0 and 1500 Gauss. The measurements were made at room temperature, again involving 100 mW laser excitation at 532 nm. The visible emission transmitted by a long pass filter at 615 nm was detected by a Si detector, and the weakness of the infrared emission meant that this signal was completely dominated by the $^3\text{A}_2 \leftrightarrow ^3\text{E}$ transition. The infrared signal was collected through a 1040 nm long pass filter and detected on an InGaAs detector. In this case the infrared band

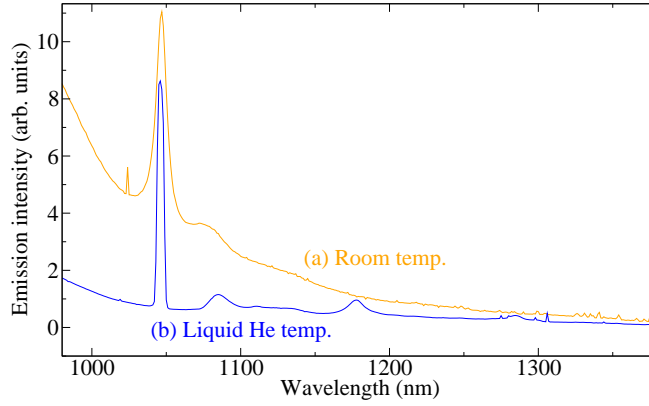


Figure 1. Infrared emission band at (a) room and (b) liquid helium temperatures for the high concentration sample with an NV^- center concentration of $3 \times 10^{18} \text{ cm}^{-3}$. Trace (b) from the cryogenic measurement has been divided by a factor of 5 on this graph in order to compensate for the enhanced ZPL intensity. The vibronic tail of the characteristic NV^- visible emission is apparent under the infrared band.

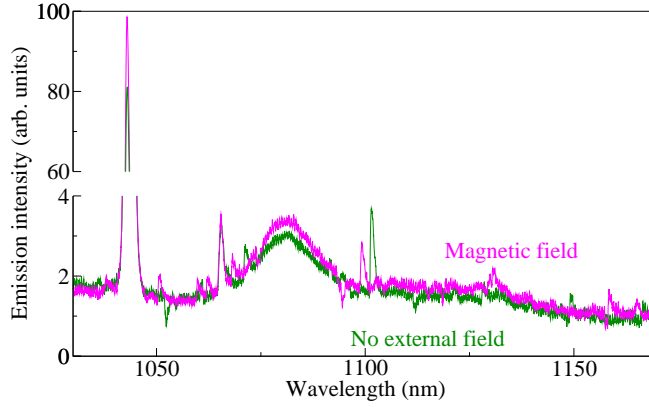


Figure 2. Infrared emission band for low concentration (10^{17} cm^{-3}) sample at liquid helium temperature. The spectrum was measured with and without an approximately 600 G magnetic field applied, and the intensity with the field was 122% of the intensity with no external field. The sharp feature at 1064 nm common to both traces was due to some scatter from the 532 nm laser.

dominated, although a small contribution (10 - 15%) remained from the vibronic tail of the $^3A_2 \leftrightarrow ^3E$ transition. Spectrally isolating the emission bands gave a more reliable measure of the change in emission magnitude with magnetic field, and this is shown in Figures 2 and 4.

High field Zeeman measurements of the 1046 nm line were also undertaken. These were made for the low concentration sample cooled to 4.2 K where the linewidth was 0.3 nm. The sample was mounted within the core of a super-conducting Helmholtz coil, and the magnetic field and 532 nm laser were directed along the $\langle 110 \rangle$ direction. The infrared emission was detected at right angles along the $\langle 100 \rangle$ direction, and the ZPL spectrum for a 5 T field is shown in Figure 5. No Zeeman shift or splitting was

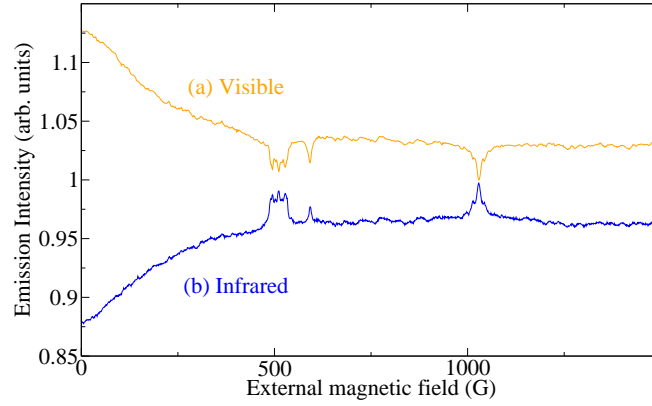


Figure 3. Emission intensity for varying external magnetic field. The field was aligned to a $\langle 111 \rangle$ crystal axis to within 0.025° . The magnetic field spectra are shown on the same scale, however the infrared intensity was many orders of magnitude weaker than that of the visible.

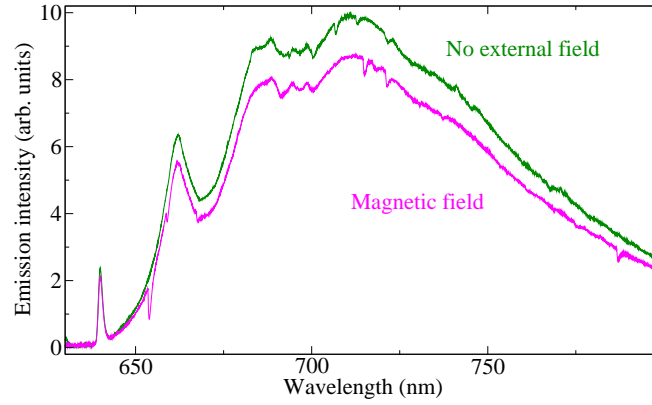


Figure 4. Change in the visible emission intensity due to presence of an approximately 600 G external magnetic field. Across the entire band, the intensity with the field was 87.7% of the intensity with no magnetic field.

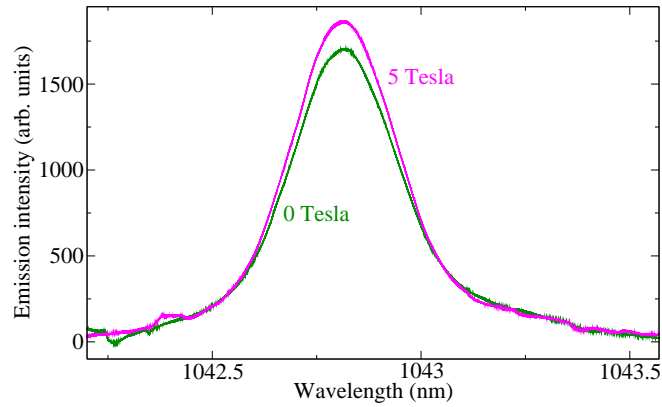


Figure 5. Infrared ZPL for 5 T magnetic field and zero field for sample at 4.2 K.

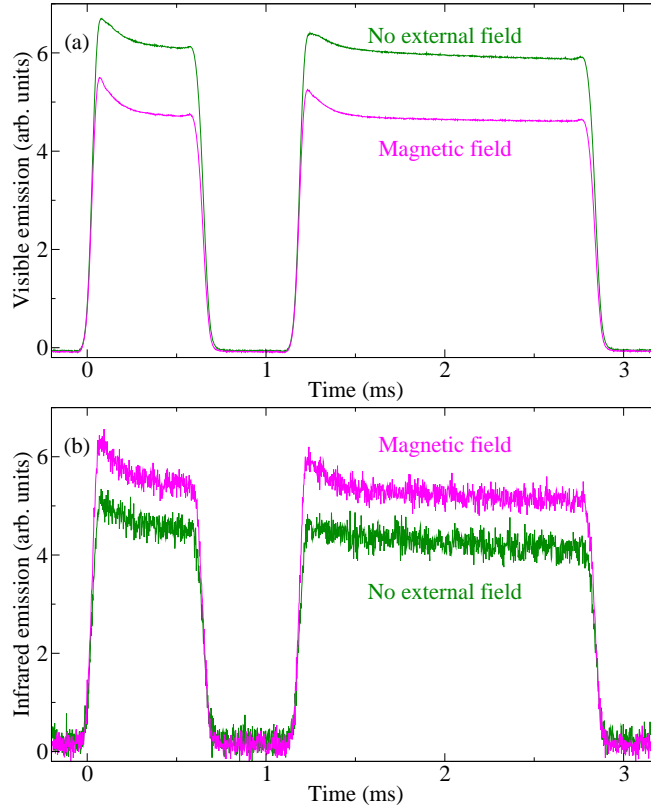


Figure 6. Visible (a) and infrared (b) emission for a 700 ns, 1700 ns pulse pair. Measured with and without a magnetic field of approximately 600 Gauss applied.

observed, although there was a small change in intensity consistent with the room temperature measurements.

2.3. Transient response

The time dependence of the infrared and visible emission was investigated for high intensity excitation pulses. Measurements were made with the sample at room temperature being excited by a focused 532 nm laser gated by an acousto-optic modulator. The emission was detected using long pass filters at 615 nm and 1000 nm for the visible and infrared, respectively, and to ensure consistency between measurements an InGaAs detector was used in both cases. The pulse sequence consisted of excitation for 700 ns, followed by a dark delay of 500 ns, and then a slightly longer second pulse of 1700 ns. The measurements were repeated with an approximately 600 Gauss field applied to the sample in a random direction. The responses are shown in Figure 6.

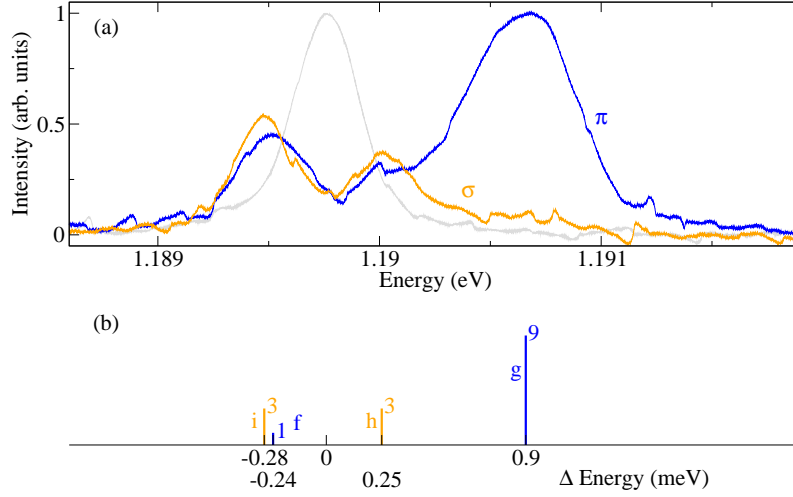


Figure 7. (a) Emission spectra for approximately 0.3 GPa stress applied along the $\langle 110 \rangle$ direction, measured along the $\langle 110 \rangle$ direction with polarization parallel (π) and perpendicular (σ) to stress. The zero stress ZPL is shown in grey for reference. (b) Theoretical patterns for an $A \leftrightarrow E$ transition at a site of C_{3v} symmetry, showing the predicted relative intensities of each line. The splittings are related to the stress coefficients of [15] by $\Delta E_i = A_1 + A_2 + C - B$; $\Delta E_f = A_1 + A_2 - C + B$; $\Delta E_h = A_1 - A_2 + C + B$; $\Delta E_g = A_1 - A_2 - C - B$. Values for these coefficients were obtained from the measured splitting of the infrared ZPL and are given in Table 1.

2.4. Uniaxial stress

The techniques of uniaxial stress spectroscopy [13, 14, 15] were used here to study the zero phonon line at 1046 nm. The low concentration 2 mm cubic sample was held at a temperature of 4.2 K while being compressed by a piston to pressures up to 0.7 GPa. Excitation was at 532 nm in the vibronic band of the ${}^3A_2 \leftrightarrow {}^3E$ transition with polarization parallel to the stress. The emission at right angles was detected with the polarization in the π (parallel to axis of stress) and σ (perpendicular to axis of stress) directions. Spectra of the 1046 nm zero phonon line were recorded for stresses along the $\langle 110 \rangle$ and $\langle 100 \rangle$ axes, and these are shown in Figures 7 and 8. Three distinct lines were observed in the spectrum taken for the $\langle 110 \rangle$ stress (although the lowest energy line could be two overlapping lines), and two for the $\langle 100 \rangle$ stress. The splitting of the 637 nm ZPL was measured, but only used to calibrate the stress and so is not shown here.

For stress along $\langle 100 \rangle$, measurements were repeated at 43 K, and the results are included in Figure 8. The figure shows that there was no thermal variation in the emission spectra over this temperature range.

3. Discussion

3.1. Energy scheme for C_{3v}

The low lying electronic states of the NV center have been considered in previous publications [12, 16]. The levels can be obtained by considering the one electron

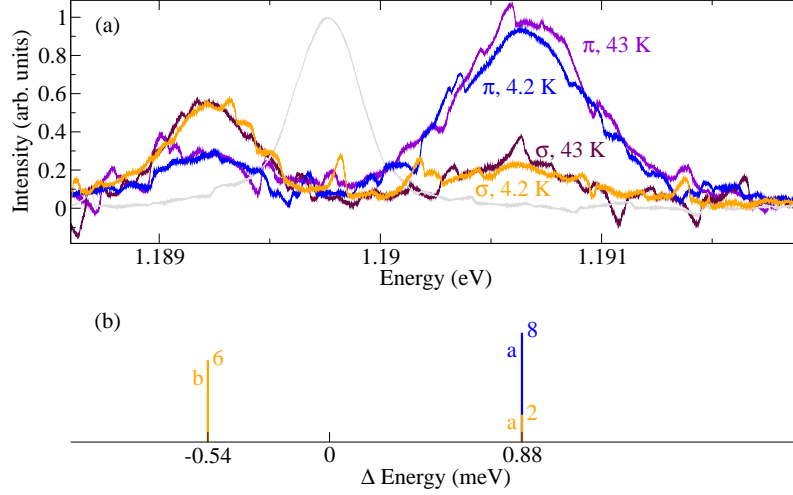


Figure 8. (a) Emission spectra for approximately 0.70 GPa stress along $\langle 100 \rangle$, measured along the $\langle 110 \rangle$ direction with polarization parallel (π) and perpendicular (σ) to stress. The zero stress ZPL is shown in grey for reference. (b) Theoretical patterns predicted for an $A \leftrightarrow E$ transition at a site of C_{3v} symmetry, where the splittings are related to the stress coefficients of [15] by $\Delta E_b = A_1 + 2B$ and $\Delta E_a = A_1 - 2B$.

states at the vacancy site adjacent to the nitrogen. In the notation for C_{3v} point group symmetry there are two one-electron orbits transforming as an A_1 irreducible representation (a_1, a'_1) and one transforming as an E irreducible representation (e), and their energies are considered to be in that order [17]. In the case of the NV^- center there are six electrons occupying these orbits and the lowest energy configuration is $a_1^2 a'_1^2 e^2$. This configuration gives rise to 3A_2 , 1A_1 , and 1E states, whereas there is a higher energy excited triplet 3E and singlet 1E associated with an $a_1^2 a'_1 e^3$ configuration. The low lying states are, therefore, as shown in black in Figure 9.

The ground state is the 3A_2 and the characteristic strong optical transition at 637 nm is from this ground state to the 3E excited state. There is fine structure associated with both of the triplet levels. In the ground state the spin levels are split by spin-spin interaction into a non-degenerate $M_s = 0$ level and a degenerate $M_s = \pm 1$ level. The excited state is split by diagonal spin-orbit interaction $\lambda L_z S_z$ into three equally spaced doubly degenerate levels and there are small displacements from the non-diagonal spin-orbit interaction, $\lambda(L_+ S_- + L_- S_+)$ [12]. What is more important for this work is the effect of spin-orbit interaction between the triplet and singlet levels. The interaction causes mixing of states transforming as the same irreducible representation, and states mixed in this way are indicated by curved arrows in Figure 9. The mixing can enable radiative or non-radiative transfer between the triplet and singlet levels, and calculation indicates that in the case of the excited 3E state the transfer will be predominantly out of $M_s = \pm 1$ levels. This is significant as it provides an alternative decay path to the visible emission. As a consequence the visible emission associated with $M_s = \pm 1$ spins is weaker than that for $M_s = 0$.

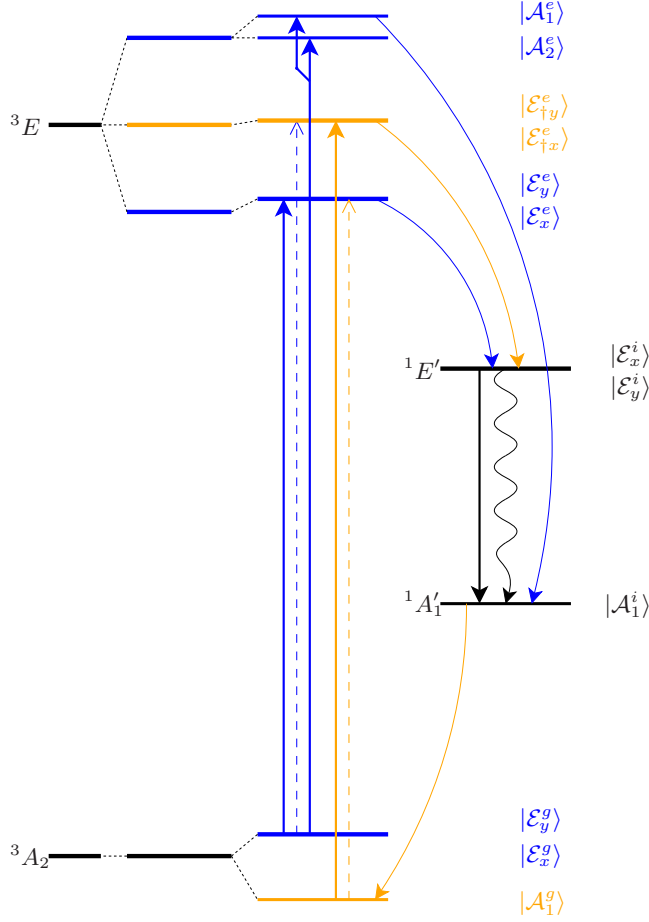


Figure 9. The energy levels expected from consideration of the one-electron states for the six NV^- electrons in C_{3v} symmetry are shown in black (first and fourth columns). Diagonal spin-orbit terms split the 3E level as shown in the second column, and spin-spin interactions give rise to the splittings in the third column. Straight arrows indicate optical transitions, and the dashed lines illustrate weakly allowed transitions that prevent perfect spin polarisation. The curved lines show symmetry-allowed inter-system crossing transitions, and the wavy line shows suspected vibronic decay between the singlets. The states are labeled on the left and the symmetry transformation properties of the spin-orbit wavefunctions are given on the right.

3.2. Magnetic field

Optical excitation causes preferential population of the $M_s = 0$ spin projection and the visible emission associated with this spin is stronger than that for $M_s = \pm 1$. Thus, as population is transferred to the $M_s = 0$ spin state the visible emission increases in intensity and, conversely, if the spin polarization is reduced the emission intensity will diminish. A static magnetic field mixes the ground state spin levels and inhibits population transfer to $M_s = 0$, reducing the spin polarisation. Varying the field strength alters the amount of mixing between levels which changes the intensity of

emission, and this effect is particularly noticeable for an axial field of 1028 Gauss. At this field value there is a complete mixing of $M_s = -1$ and $M_s = 0$ states. The population will be equally distributed between the two spins whereas it will be almost entirely in $M_s = 0$ at adjacent magnetic field values. Thus an axially aligned magnetic field swept through 1028 Gauss causes a marked reduction in population and noticeable drop in the visible emission intensity as seen in trace (a) of Figure 3. With the reduction of spin polarisation there is an increase in the $M_s = -1$ population, which increases the transfer rate to the singlet levels and should increase the emission intensity from any optical transitions within the alternative decay path. Exactly such a rise is observed in the infrared emission at 1028 Gauss.

All the other intensity variation of the visible emission in Figure 3 can be similarly explained by variation in the spin polarization of the NV^- centre. For example, at the special cases of axial fields at 514 Gauss and 660 Gauss there is cross relaxation between the NV^- centre aligned with the field and other spin systems in the crystal (single substitutional nitrogen defects and non-aligned NV^- centres, respectively) [18, 19]. These other spin systems are not spin polarised and the cross relaxation will hence reduce the polarisation of the NV^- centre, causing the visible emission to diminish.

It is immediately apparent from Figure 3 that the infrared emission contains the same features, and two conclusions can be drawn. Firstly, the complete (anti-) correlation of this intensity with that of the visible emission (which varies due to NV^- spin polarisation) proves the new emission band is associated with the NV^- centre. Secondly, the fact that it is anti-correlated shows the infrared emission is associated with the population involved in the inter-system crossing.

High magnetic fields were experimentally found not to split the infrared zero-phonon line. Although this rules out the possibility of the emission arising from certain transitions, subtleties mean that it does not conclusively identify the correct transition. A triplet-triplet cannot immediately be eliminated, as it is already known that the $^3A_2 \leftrightarrow ^3E$ (637 nm) zero-phonon line is not split by a magnetic field [10, 20]. The individual levels of the triplets are split, but the optical transitions are between levels of like spin and so they remain degenerate, as shown in Figure 10. The same could occur for the infrared, but this option can be dismissed as there are no other triplet levels in the NV^- system. Unlike triplet levels, spin-singlets are not split by a magnetic field, and thus Zeeman splitting of the ZPL would be expected in general for a triplet-singlet transition. A subtlety here is that no splitting would be observed if the transition were restricted to a particular spin level of the triplet state, as is indicated in Figure 10 for the transition that feeds back to the ground state. However this diagram is accurate for an axially aligned field only, and the four different NV^- orientations in a bulk diamond sample makes it impossible to achieve total alignment. Mixing between spin levels in misaligned centres would lead to observable splitting.

To first order, no splitting would occur for a singlet-singlet transition. It is possible for orbitally degenerate states to separate and give rise to some spectral broadening or splitting, but this can be expected to be too small to result in a measurable splitting (as it is for the $^3A_2 \leftrightarrow ^3E$ transition). The experimental result in Figure 5 is most consistent with the infrared emission arising from the $^1E \leftrightarrow ^1A_1$ singlet-singlet transition.

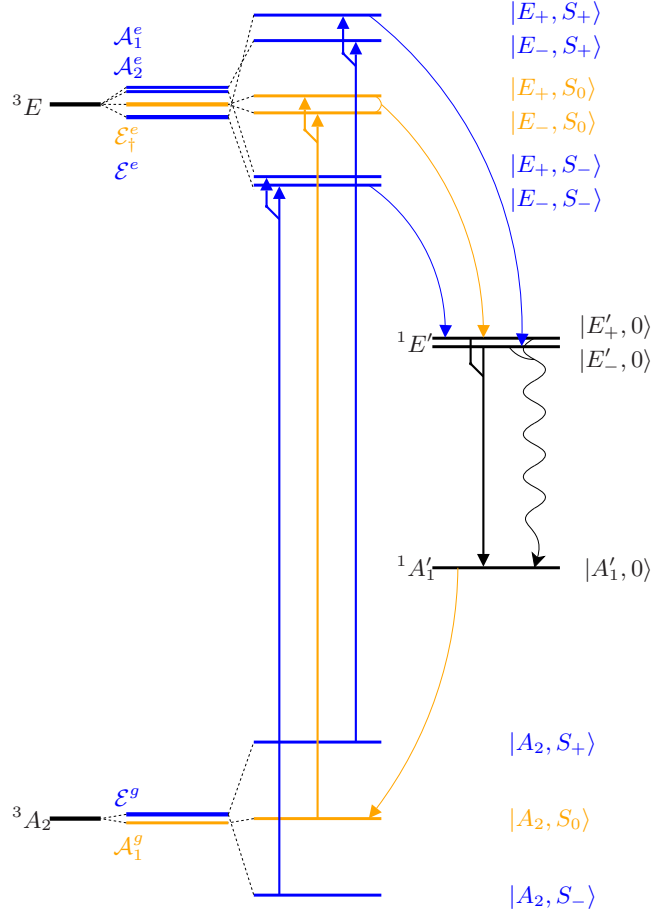


Figure 10. Theoretical energy levels for a high (axial) magnetic field situation are shown in the third column. The first two columns contain the spin-orbit levels that are shown in detail in Figure 9. Straight arrows indicate optical transitions, curved lines show symmetry-allowed inter-system crossing transitions, and the wavy line shows suspected vibronic decay between the singlets. The wavefunctions in the presence of a large field are given on the right.

3.3. Transients

The response of the visible emission to intense excitation pulses has been interpreted previously [12]. Initially the NV^- centres are evenly distributed between the three spin projections and they are excited equally. With excitation, the spin-selective inter-system crossing preferentially populates the $M_s = 0$ level and causes spin polarisation as has already been discussed. This increase in spin polarisation typically increases the visible emission intensity, however for intense excitation (as used here) an equilibrium population is built up in a long-lived (300 ns) “storage” state in the singlet system. This decreases the population that contributes to the visible emission, causing the drop in visible emission occurring over the first few hundred ns that is prominent in Figure 6. At the start of the second pulse the population is still spin polarised and so the inter-system crossing is slightly slower. This is observed as a reduction in the rate

that the emission drops to its equilibrium intensity (ie the storage singlet builds up an equilibrium population). The peak at the beginning of the second pulse is lower than that of the first, as some population remains in the storage level after the 500 ns delay and some population is lost through photoionization [21].

The situation is changed by a weak magnetic field, which causes a mixing of the ground state spin levels and prevents spin polarisation. As a result, more population takes the alternative decay path through the singlet levels and a larger equilibrium population is maintained in the storage state. Thus the visible emission intensity is lower than it was without the magnetic field. Since the difference between the first and second pulses was explained by residual spin polarisation, both pulses should be identical in the case of a magnetic field. In the experiment, the observed difference that does occur between pulses is due to imperfect quenching of spin polarisation and also to photoionization [21].

Comparing the infrared and visible responses to excitation pulses in Figure 6, it is immediately obvious that there is much similarity. The major difference is that the magnetic field increases the infrared intensity whereas it decreases the visible, which is consistent with the magnetic field spectra discussed above. However, the drop in infrared emission intensity within the first few hundred nanoseconds of each pulse (similar to that obtained in the visible) indicates that the emitting level is not the “storage” level. This confirms that the infrared band is emitted from the ${}^1E \rightarrow {}^1A_1$ singlet-singlet transition, and suggests that the lower singlet state is the 300 ns storage level. Such a conclusion is plausible, as the upper singlet could lie close to the excited triplet state to enable efficient inter-system crossing and the lower singlet could then be several hundred meV (1000s of cm^{-1}) above the ground state with much slower inter-system crossing. Attempts were made to re-pump the singlet-singlet transition by exciting in the infrared to confirm this analysis, but they have not been successful. We were, therefore, not able to establish where the singlet levels lie in relation to the triplet levels.

The responses in Figure 6 provide additional lifetime information. The rates of emission decay from the initial intensity for each excitation pulse are similar for the visible and infrared, indicating similar dynamics. The excited state lifetime for the visible emission is known to be about 12 ns [22, 23], and the signal contrast ratio between spin polarised and unpolarised (as can be seen in Figures 2 and 4) indicates that population from the excited triplet crosses to the singlet system at a similar rate. Thus the population must not spend extra little time in the upper singlet level before giving the infrared emission. However, a singlet-singlet transition is unlikely to be appreciably stronger than an allowed triplet-triplet transition and the most likely explanation for this short lifetime is that there is also competing non-radiative decay between the singlet levels as indicated by the wavy line in Figures 9 and 10. Significant non-radiative decay would account for both the short lifetime and the weakness of the emission. This may be a general phenomenon for transitions in the infrared as there are few reports of diamond emitting at these wavelengths [24]. Such an increased contribution of non-radiative decay at low-energy transitions in diamond can be attributed to the strong electron phonon coupling and high vibrational frequencies.

In summary, the following physical description is consistent with the data. There is an almost 50% branching of the population from the 3E to the singlets, and the upper singlet has a short lifetime (< 1 ns) mainly due to non-radiative decay. The lower singlet level has a longer lifetime (≈ 300 ns) identified previously [12].

Table 1. Stress coefficients for the visible and infrared transitions. The values for the visible are from [25], with the signs of B and C adjusted to reflect the convention in [26] adopted here.

	Visible ($\times 10^{-12}$ eV Pa $^{-1}$)	Infrared ($\times 10^{-12}$ eV Pa $^{-1}$)
A_1	1.47	0.53
A_2	-3.85	-1.44
B	-1.04	-0.51
C	-1.69	-0.58

3.4. Uniaxial stress measurements

The splitting of the zero phonon line with uniaxial stress can be used to determine the symmetry of the states involved in optical transitions. A study of this type was undertaken by [25] and they showed the 637 nm zero-phonon line to be associated with an $A \leftrightarrow E$ transition at a site of trigonal symmetry. In the present work this $A \leftrightarrow E$ transition was excited, but energy transferred within the NV^- system gives rise to the infrared transition which was investigated.

For stress applied along a $\langle 110 \rangle$ direction, two pairs of NV centres have equivalent orientations and both pairs are excited. In all cases there is a component of strain perpendicular to the NV^- axis and for an $A \leftrightarrow E$ transition a maximum of four lines is therefore predicted [25, 26]. This is consistent with the experimental observation shown in Figure 7, and the polarization pattern for an $A \leftrightarrow E$ transition shown below the experimental traces is also in plausible correspondence. Some deviation of the polarisation pattern is likely to be due to loss of polarization from scatter from the crystal faces, as they were not optically polished.

Parameters for the stress splitting of an $A \leftrightarrow E$ transition in trigonal symmetry were introduced by [15], and their values for the present transition were calculated from the energy splittings of the four lines in Figure 7 and are given in Table 1. They are of the order of a factor 2.5 smaller than those for the 637 nm zero phonon line determined for by [25]. The small values for the strain parameters and the small value for the inhomogeneous linewidth are consistent with a transition such as ${}^1E(a_1^2 a_1'^2 e^2) \leftrightarrow {}^1A_1(a_1^2 a_1'^2 e^2)$, which involves a spin change but no change of orbit between initial and final state.

For a stress along the $\langle 100 \rangle$ direction all four NV^- orientations are at the same angle to the stress and the excitation polarisation. Each orientation is thus equally excited, and for an $E \rightarrow A$ transition the component of strain perpendicular to the NV^- axes would lift the degeneracy of the excited E state. The splitting would be the same for all orientations, and so produce two lines. The spectra for $\langle 100 \rangle$ stress shown in Figure 8 is consistent with this description, and there is plausible correspondence with the expected polarization pattern shown below the experimental traces.

Since the spin polarisation is to the $M_s = 0$ level of the ground state, and this spin level transforms with A_1 symmetry as indicated in Figure 9, the 1A_1 state should be the lower of the singlet states [12]. With the 1E as the upper level, the Boltzmann population distribution of the split components might be expected to change with temperature. This would cause a change in the relative intensities of the lines in the spectrum, but no such change was observed between a temperature of 4.2 and 43 K (Figure 8). In Section 3.3 it was argued that the lifetime of this upper singlet is

very short, and it is possible that there is insufficient time to establish a Boltzmann distribution.

4. Conclusion

An emission band has been observed in the infrared, with a zero phonon line at 1046 nm. Measurements have established that this infrared emission is associated with the NV^- defect centre, which has previously been investigated through its well documented visible transition at 637nm. From theoretical considerations, magnetic field and uniaxial stress measurements the infrared emission is attributed to a $^1A_1 \leftrightarrow ^1E$ transition where these singlet levels lie between the ground and excited state triplets. Although the results presented here are consistent with the 1E being the higher of the singlets, the order of the levels has not been conclusively established. Some contention over the order of these singlet levels already exists due to previous numerical calculations [27, 28].

There are some further puzzling features about the infrared emission that remain unresolved. The documented energies of the vibrational sidebands associated with the visible transition (66 and 140 meV [29]) are not matched by the infrared sideband energies (42.6, 133 and 221 meV). The first of these is very small and the last is large, well outside the range of single phonons in diamond. The origin of these frequencies is unclear but the small electron-phonon coupling, as well as the small stress parameters and inhomogeneous line width, are consistent with theoretical models of a transition involving only a spin reorientation. Another strange aspect is the weakness of the infrared emission. The inter-system crossing branching ratio is as high as 50% for the $M_s = \pm 1$ spin state but yet the infrared emission is orders of magnitude weaker than that of the visible emission. The explanation that has been advanced is that there is also very significant non-radiative decay for the same transition. Related to this is that with emission arising almost exclusively from $M_s = \pm 1$ spins then it is surprising that it only drops 15% with spin polarization. It suggests that the level of spin polarization attained in our the samples was very small.

Despite these issues, the observation of the singlet to singlet transitions adds significantly to our understanding of the electronic structure of the NV centre. It provides a new avenue whereby the centre, and in particular the process of spin polarisation, can be studied and used for quantum information processing applications.

Acknowledgments

This work has been supported by Australian Research Council.

References

- [1] F Jelezko and J Wrachtrup. Read-out of single spins by optical spectroscopy. *J. Phys. Condens. Matter*, 16:R1089–R1104, 2004.
- [2] F. Jelezko, T. Gaebel, I. Popa, M. Domhan, A. Gruber, and J. Wrachtrup. Observation of coherent oscillation of a single nuclear spin and realization of a two-qubit conditional quantum gate. *Phys. Rev. Lett.*, 93(13):130501, 2004.
- [3] L. Childress, M. V. Gurudev Dutt, J. M. Taylor, A. S. Zibrov, F. Jelezko, J. Wrachtrup, P. R. Hemmer, , and M. D. Lukin. Coherent dynamics of coupled electron and nuclear spin qubits in diamond. *Science*, 314:281, 2006.
- [4] Jörg Wrachtrup and Fedor Jelezko. Processing quantum information in diamond. *J. Phys. Condens. Matter*, 18:S807–S824, 2006.

- [5] R. Hanson, O. Gywat, and D. D. Awschalom. Room-temperature manipulation and decoherence of a single spin in diamond. *Phys. Rev. B*, 74(16):161203, 2006.
- [6] Torsten Gaebel, Michael Domhan, Iulian Popa, Christoffer Wittmann, Philipp Neumann, Fedor Jelezko, James R. Rabeau, Nikolas Stavrias, Andrew D. Greentree, Steven Prawer, Jan Meijer, Jason Twamley, Philip R. Hemmer, and Jorg Wrachtrup. Room-temperature coherent coupling of single spins in diamond. *Nature Physics*, 2:408, June 2006.
- [7] C. Santori, D. Fattal, S. M. Spillane, M. Fiorentino, R. G. Beausoleil, A. D. Greentree, P. Olivero, M. Draganski, J. R. Rabeau, P. Reichart, B. C. Gibson, S. Rubanov, D. N. Jamieson, , and S. Prawer. Coherent population trapping in diamond n-v centers at zero magnetic field. *Opt. Express*, 14:7986–7993, 2006.
- [8] F.C. Waldermann, P. Olivero, J. Nunn, K. Surmacz, Z.Y. Wang, D. Jaksch, R.A. Taylor, I.A. Walmsley, M. Draganski, P. Reichart, A.D. Greentree, D.N. Jamieson, and S. Prawer. Creating diamond color centers for quantum optical applications. *Diamond Relat. Mater.*, 16:1887 – 1895, November 2007.
- [9] J.H.N. Loubser and J.A. Van Wyk. Optical spin-polarisation in a triplet state in irradiated and annealed type 1b diamonds. *Diamond Res.*, 1:11–15, 1977.
- [10] N. R. S. Reddy, N. B. Manson, and E. R. Krausz. Two-laser spectral hole burning in a colour centre in diamond. *J. Lumin.*, 38:46, December 1987.
- [11] D. A. Redman, S. Brown, R. H. Sands, and S. C. Rand. Spin dynamics and electronic states of n-v centers in diamond by epr and four-wave-mixing spectroscopy. *Phys. Rev. Lett.*, 67(24):3420–3423, Dec 1991.
- [12] N. B. Manson, J. P. Harrison, and M. J. Sellars. Nitrogen-vacancy center in diamond: Model of the electronic structure and associated dynamics. *Phys. Rev. B*, 74(10):104303, 2006.
- [13] A A Kaplyanskii. *Opt. Spectrosc.*, 16:329–337, 1964.
- [14] A A Kaplyanskii. *Opt. Spectrosc.*, 16:557–565, 1964.
- [15] A E Hughes and W A Runciman. Uniaxial stress splitting of doubly degenerate states of tetragonal and trigonal centres in cubic crystals. *Proc. Phys. Soc.*, 90:827–838, 1967.
- [16] N B Manson and R L McMurtrie. Issues concerning the nitrogen-vacancy center in diamond. *J. Lumin.*, 127:98–103, 2007.
- [17] A. Lenef and S. C. Rand. Electronic structure of the n-v center in diamond: Theory. *Phys. Rev. B*, 53(20):13441–13455, May 1996.
- [18] K Holliday, N B Manson, M Glasbeek, and E van Oort. Optical hole-bleaching by level anti-crossing and cross relaxation in the n-v centre in diamond. *J. Phys. Condens. Matter*, 1(39):7093–7102, 1989.
- [19] R. J. Epstein, F. M. Mendoza, Y. K. Kato, and D. D. Awschalom. Anisotropic interactions of a single spin and dark-spin spectroscopy in diamond. *Nature Physics*, 1:94–98, 2005.
- [20] H. Hanzawa, H. Nishikori, Y. Nisida, S. Sato, T. Nakashima, S. Sasaki, , and N. Miura. Zeeman effect on the zero-phonon line of the nv center in synthetic diamond. *Physica B: Condensed Matter*, 184:137 – 140, 1993.
- [21] N B Manson and J P Harrison. Photo-ionization of the nitrogen-vacancy center in diamond. *Diamond Relat. Mater.*, 14:1705–1710, October 2005.
- [22] A T Collins, M F Thomaz, and M I B Jorge. Luminescence decay time of the 1.945 ev centre in type 1b diamond. *J. Phys. C*, 16:2177 – 2181, 1983.
- [23] A. Batalov, C. Zierl, T. Gaebel, P. Neumann, I.-Y. Chan, G. Balasubramanian, P. R. Hemmer, F. Jelezko, and J. Wrachtrup. Temporal coherence of photons emitted by single nitrogen-vacancy defect centers in diamond using optical rabi-oscillations. *Phys. Rev. Lett.*, 100(7):077401, 2008.
- [24] Alexander M. Zaitsev. *Optical Properties of Diamond: A Data Handbook*. Springer, 2001.
- [25] Gordon Davies and M F Hamer. Optical studies of the 1.945 ev vibronic band in diamond. *Proc. R. Soc. Lond. A.*, 348:285–298, 1976.
- [26] K Mohammed, G Davies, and A T Collins. Uniaxial stress splitting of photoluminescence transitions at optical centres in cubic crystals: theory and application to diamond. *J. Phys. C*, 15:2779–2788, 1982.
- [27] J. P. Goss, R. Jones, S. J. Breuer, P. R. Briddon, and S. Öberg. The twelve-line 1.682 ev luminescence center in diamond and the vacancy-silicon complex. *Phys. Rev. Lett.*, 77(14):3041–3044, Sep 1996.
- [28] Adam Gali, Maria Fyta, and Efthimios Kaxiras. Ab initio supercell calculations on nitrogen-vacancy center in diamond: Electronic structure and hyperfine tensors. *Phys. Rev. B*, 77:155206, 2008.
- [29] Gordon Davies. Vibronic spectra in diamond. *J. Phys. C*, 7:3797–3809, 1974.